

# Evaluation of carbon monoxide oxidation over $\text{CeO}_2/\text{Co}_3\text{O}_4$ catalysts: Effect of ceria loading

Chih-Wei Tang<sup>a,b</sup>, Ming-Chih Kuo<sup>b</sup>, Chin-Jung Lin<sup>b</sup>,  
Chen-Bin Wang<sup>a,\*</sup>, Shu-Hua Chien<sup>b,c,\*\*</sup>

<sup>a</sup>Department of Applied Chemistry and Materials Science, Chung Cheng Institute of Technology,  
National Defense University, Taohsi, Taoyuan 33509, Taiwan, ROC

<sup>b</sup>Institute of Chemistry, Academia Sinica, Taipei 11529, Taiwan, ROC

<sup>c</sup>Department of Chemistry, National Taiwan University, Taipei 10764, Taiwan, ROC

Available online 26 November 2007

## Abstract

Modification of cobaltic oxide (obtained from the reduction of high-valence cobalt oxide and assigned as R230,  $S_{\text{BET}} = 100 \text{ m}^2 \text{ g}^{-1}$ ) with different loading of ceria was proceeded using the impregnation method (assigned as  $\text{CeX/R230}$ ,  $X = 4, 12, 20, 35$  and  $50 \text{ wt}\%$ ). The  $\text{CeX/R230}$  catalysts were characterized by X-ray diffraction (XRD), nitrogen adsorption at  $-196 \text{ }^\circ\text{C}$ , temperature-programmed reduction (TPR) and transmission electron microscopy (TEM). Their catalytic activities towards the CO oxidation were studied in a continuous flow micro-reactor. The results revealed that the optimal modification, i.e.,  $\text{Ce20/R230}$ , can increase the surface area ( $S_{\text{BET}} = 109 \text{ m}^2 \text{ g}^{-1}$ ) of cobaltic oxide, further weaken the bond strength of Co–O and lower the activation of CO oxidation among  $\text{CeX/R230}$  catalysts due to the combined effect of cobaltic oxide and ceria. The  $\text{Ce20/R230}$  catalyst exhibited the best catalytic activity in CO oxidation with  $T_{50}$  (temperature for 50% CO conversion) at  $88 \text{ }^\circ\text{C}$ .

© 2007 Elsevier B.V. All rights reserved.

**Keywords:** Ceria; Cobaltic oxide; CO oxidation

## 1. Introduction

Highly active catalysts for CO oxidation have several applications including vehicle exhausts [1], gas sensor [2], catalytic combustion [3] and magnetic material [4]. Many catalysts have been designed and tested for CO oxidation under low temperature. For instance, noble metal catalysts, such as  $\text{Au/Co}_3\text{O}_4$ ,  $\text{Au}/\alpha\text{-Fe}_2\text{O}_3$ ,  $\text{Au/MnO}_x$ ,  $\text{Pt/SnO}_2$ ,  $\text{Pd/SnO}_2$  have been demonstrated to be very effective in CO oxidation [5–7].

The high cost of precious metals and their sensitivity to sulfur poisoning have long motivated the search for substitute catalysts. As a single component, base metal catalysts cannot compete with precious metal catalysts, and attempts have been made to improve their activity by combining various elements. The availability of metal oxides is such that attention has been paid on

especially cerium oxide [8–13], cobalt oxide [14–19] and  $\text{Co}_3\text{O}_4/\text{CeO}_2$  binary oxide [20,21]. Ceria has a high oxygen storage capacity and has well-known catalytic and redox properties with coupled of ( $\text{Ce}^{4+}/\text{Ce}^{3+}$ ), making more oxygen available for the oxidation process. It is well known that  $\text{CeO}_2$  is a promoter additive. The most important property comes from the oxygen storage and releasing capacity on  $\text{CeO}_2$  that promotes CO oxidation and  $\text{NO}_x$  reduction. Both  $\text{Co}_3\text{O}_4$  and  $\text{CoO}$  are stable oxides in the cobalt oxide system [15,22,23]. The high activity of  $\text{Co}_3\text{O}_4$  is likely to be related to the relatively low  $\Delta H$  of vaporization of  $\text{O}_2$  [22]. Therefore, the Co–O bond strength of  $\text{Co}_3\text{O}_4$  can affect the desorption of lattice oxygen. The oxidation of carbon monoxide on various composites of metal oxides was investigated. Under the conditions of ambient temperature,  $\text{GHSV} = 15,000 \text{ h}^{-1}$  and  $1\% \text{ CO}/21\% \text{ O}_2/78\% \text{ He}$ , Shen et al. [20,21] found that the prepared mixed oxides by the coprecipitation–oxidation method with large surface area exhibited the high activity (complete conversion) and stability (maintained 2400 min) for CO oxidation. Also, our previous research [23] finds that the  $\text{CeO}_2/\text{Co}_3\text{O}_4$  catalyst possesses superior activity than other catalysts.

\* Corresponding author.

\*\* Corresponding author at: Department of Chemistry, National Taiwan University, Taipei 10764, Taiwan, ROC.

E-mail addresses: [chenbin@ccit.edu.tw](mailto:chenbin@ccit.edu.tw) (C.-B. Wang), [chiensh@gate.sinica.edu.tw](mailto:chiensh@gate.sinica.edu.tw) (S.-H. Chien).

This study is concerned with the effect of ceria loading for the oxidation of carbon monoxide over  $\text{CeO}_2/\text{Co}_3\text{O}_4$  catalysts. The purpose is to find the optimized loading of ceria for this composite catalyst that abates the CO under low temperature.

## 2. Experimental

### 2.1. Catalyst preparation

The detailed high-valence cobalt oxide (marked as  $\text{CoO}_x$ ) prepared procedure has been described in a previous investigation [24]. Moreover, the pure cobaltic oxide ( $\text{Co}_3\text{O}_4$ ) was refined from  $\text{CoO}_x$  by a controlled hydrogen reduction in a temperature-programmed reduction system to 230 °C (assigned as R230). Modification of cobaltic oxide was further proceeded by impregnating the R230 with a series of cerium nitrate solutions (assigned as  $\text{CeX/R230}$ ,  $X = 4, 12, 20, 35$  and 50 wt%). Then, prepared samples were dried overnight in an oven at 110 °C, and then reduced in 10%  $\text{H}_2/\text{Ar}$  for 1 h at 200 °C.

### 2.2. Catalyst characterization

X-ray diffraction (XRD) measurements were made using a Siemens D5000 diffractometer with  $\text{Cu K}\alpha_1$  radiation ( $\lambda = 1.5405 \text{ \AA}$ ) at 40 kV and 30 mA with a scanning speed in  $2\theta$  of  $2^\circ \text{ min}^{-1}$ . Diffraction peaks of the crystalline phase were compared with those of standard compound reported in the JCPDS data files ( $\text{Co}_3\text{O}_4$ : 34-0394;  $\text{CeO}_2$ : 09-0418). The crystallite sizes of cobaltic oxide and ceria were calculated using the Scherrer equation.

Nitrogen adsorption isotherms at  $-196^\circ\text{C}$  were determined volumetrically with Micromeritics ASAP 2010. The catalysts were pre-outgassed under  $5 \times 10^{-5}$  Torr and 110 °C for 3 h. The surface area of samples was determined from the nitrogen adsorption isotherm.

Reduction behavior of  $\text{CeX/R230}$  catalysts was investigated by temperature-programmed reduction (TPR). About 25 mg of the sample was heated in a flow of 10%  $\text{H}_2/\text{He}$  gas mixture at a flow rate of  $10 \text{ ml min}^{-1}$ . During TPR, the temperature was programmed to rise with  $10^\circ\text{C min}^{-1}$  to 550 °C.

Cobalt oxides microstructures were characterized using TEM (Hitachi H600-3). The samples for the electron microscopy were prepared by making an ethanol suspension and deposited onto an undercoat of a holey carbon film.

### 2.3. Catalytic activity measurement

The catalytic activities of  $\text{CeX/R230}$  catalysts towards CO oxidation were measured in a continuous flow micro-reactor. The reaction gas, a mixture of 10%  $\text{O}_2/\text{He}$  with 4%  $\text{CO}/\text{He}$ , was fed to a 0.5 g catalyst at a rate of  $20 \text{ ml min}^{-1}$ . Steady-state catalytic activity was measured at each temperature with the reaction temperature raised from room temperature to 200 °C in steps of 25 °C. The effluent gas was analyzed on-line using a Varian 3700 gas chromatograph with a carboxsphere column. Before the reaction, the catalyst was pretreated in flowing 10%

$\text{O}_2/\text{He}$  at 110 °C for 1 h to drive away molecules that had been pre-adsorbed from the atmosphere.

## 3. Results and discussion

Fig. 1 displays the XRD patterns of the ceria, cobaltic oxide and the  $\text{CeX/R230}$  catalysts. All of the peaks of Fig. 1(a) can be indexed to the cubic phase of ceria(IV) with fluorite structure. After reduction, the  $\text{CeX/R230}$  catalysts exhibit three crystalline structures:  $\text{CeO}_2$ ,  $\text{Co}_3\text{O}_4$  and  $\text{CoO}$ , as demonstrated by XRD [Fig. 1(c)–(g)]. The diffraction peaks of ceria become stronger with the increase of loading. Observed from the width of diffraction peaks reveal that the crystallite sizes of ceria did not noticeably change.

The TPR profiles of ceria, cobaltic oxide and  $\text{CeX/R230}$  catalysts are shown in Fig. 2. The reduction of pure  $\text{CeO}_2$  initiates at 503 °C [Fig. 2(a)], and the signal is much weaker than those of  $\text{Co}_3\text{O}_4$  and  $\text{CeO}_2/\text{Co}_3\text{O}_4$  catalysts [23,25]. The peak is attributed to the removal of surface capping oxygen ions during the reduction reaction [26,27]. The reduction profile of the pure  $\text{Co}_3\text{O}_4$  can be characterized by the two consequent peaks between 200 and 400 °C [23,28]. All of the samples, except for  $\text{CeO}_2$  [Fig. 2(a)] exhibits two well-resolved reduction peaks

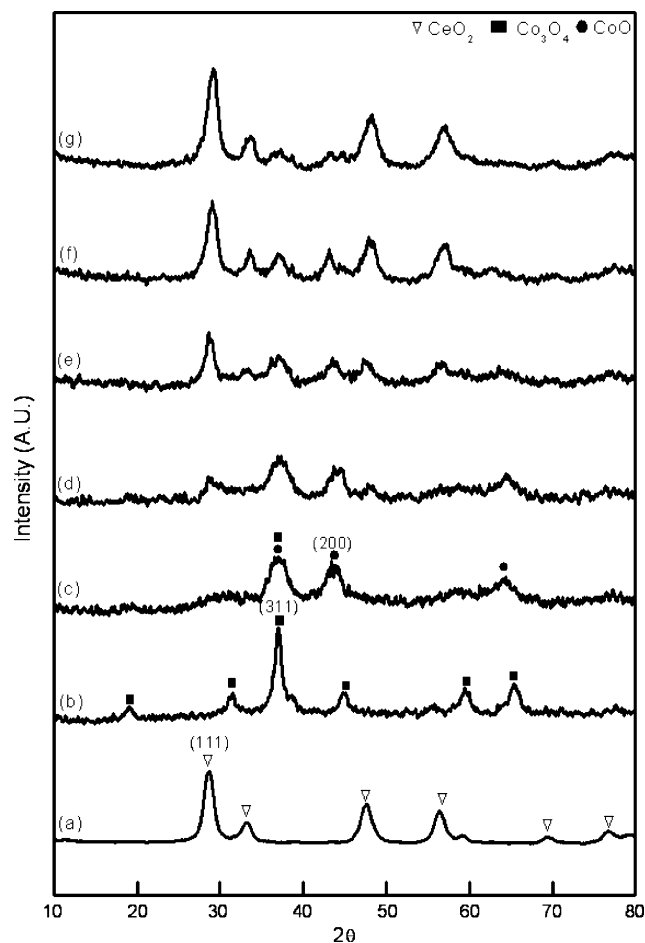


Fig. 1. XRD characterization for the ceria, cobaltic oxide and the  $\text{CeX/R230}$  catalysts: (a)  $\text{CeO}_2$ , (b) R230, (c) Ce4/R230, (d) Ce12/R230, (e) Ce20/R230, (f) Ce35/R230 and (g) Ce50/R230.

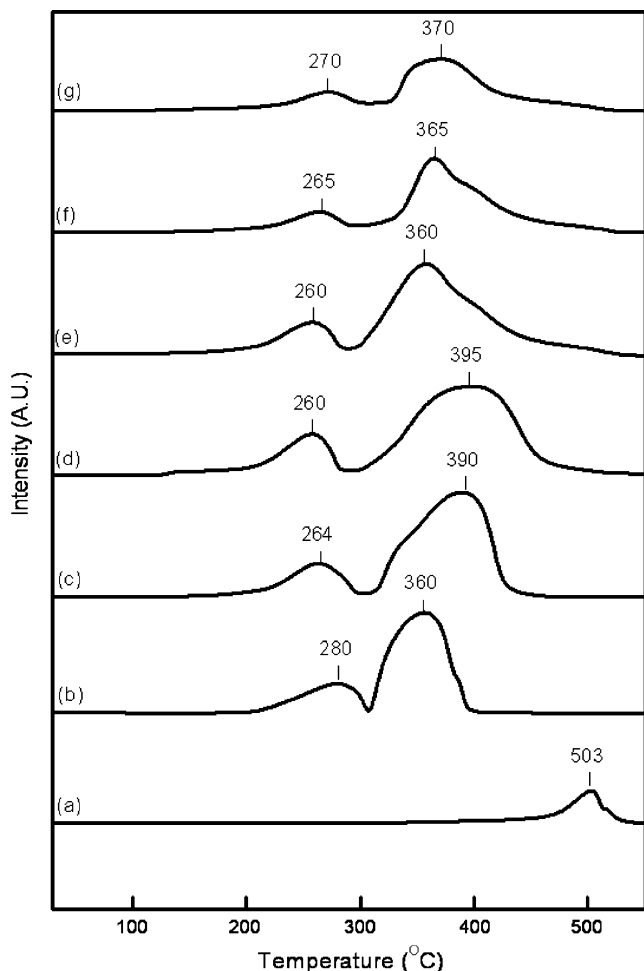


Fig. 2. TPR profiles for the ceria, cobaltic oxide and the CeX/R230 catalysts: (a) CeO<sub>2</sub>, (b) R230, (c) Ce4/R230, (d) Ce12/R230, (e) Ce20/R230, (f) Ce35/R230 and (g) Ce50/R230.

(assigned as  $\alpha$  and  $\beta$  peaks). These profiles indicate a two-step reduction process: the first peak ( $\alpha$  peak) of low intensity initiates at low temperature and overlaps with the more intense second peak ( $\beta$  peak). According to our previous reports [19,23,24], the  $\alpha$  peak is attributed to the reduction of Co<sup>3+</sup> ions, which are present in the spinel structure, into Co<sup>2+</sup> [Eq. (1)]. Subsequently, the  $\beta$  peak observes that comes from the reduction of CoO to metallic cobalt [Eq. (2)].



As shown in Fig. 2(b)–(f) and both the 3rd and 4th columns in Table 1, an apparent shift in both  $\alpha$  and  $\beta$  peaks appears which is related to the surface area of catalysts. Compared to the  $S_{\text{BET}}$  (the 2nd column of Table 1), both  $\alpha$  and  $\beta$  peaks shift to lower temperatures with the increase of  $S_{\text{BET}}$ , i.e., both  $\alpha$  and  $\beta$  peaks of Ce20/R230 sample ( $S_{\text{BET}} = 109 \text{ m}^2 \text{ g}^{-1}$ ) are found at 260 and 360 °C [Fig. 2(e)], respectively. Both  $\alpha$  and  $\beta$  peaks of Ce50/R230 sample ( $S_{\text{BET}} = 52 \text{ m}^2 \text{ g}^{-1}$ ) occurred at 272 and 370 °C [Fig. 2(g)], respectively. These results reveal that the increasing of the  $S_{\text{BET}}$  of Ce20/R230 catalysts can weaken the

Table 1

Characterization and catalytic activities for CO oxidation over CeX/R230 catalysts

Catalysts	$S_{\text{BET}}$ ( $\text{m}^2 \text{ g}^{-1}$ )	TPR (°C)		CO oxidation	
		$\alpha$	$\beta$	$E_a^a$ (kJ mol <sup>-1</sup> )	$T_{50}^b$ (°C)
Ce4/R230	71	263	390	26	108
Ce12/R230	81	260	390	18	93
Ce20/R230	109	260	360	10	88
Ce35/R230	65	266	365	31	111
Ce50/R230	52	270	370	55	127

<sup>a</sup> Calculated according to the Arrhenius equation.

<sup>b</sup> Temperature for 50% CO conversion.

bond strength of Co–O bond and can promote more lattice oxygen desorption from Co<sub>3</sub>O<sub>4</sub> to decrease the reduction temperature.

In order to understand whether the optimal addition of ceria can increase the surface area and provide oxygen storage capacity, the ratio of  $\alpha$  and  $\beta$  peaks for each CeX/R230 sample is quantitatively determined from the consumption of hydrogen in TPR traces. The amounts of hydrogen consumption with the same temperature of CeX/R230 catalysts are shown in Fig. 3. The relative area of  $\alpha$  and  $\beta$  ( $N_{\text{H}_2}/N_{\text{Co}}$  ratio) are determined to be 0.47 and 1.7; 0.43 and 1.7; 0.39 and 1.4; 0.39 and 1.4; 0.30 and 1.38, respectively, for Ce20/R230, Ce12/R230, Ce4/R230,

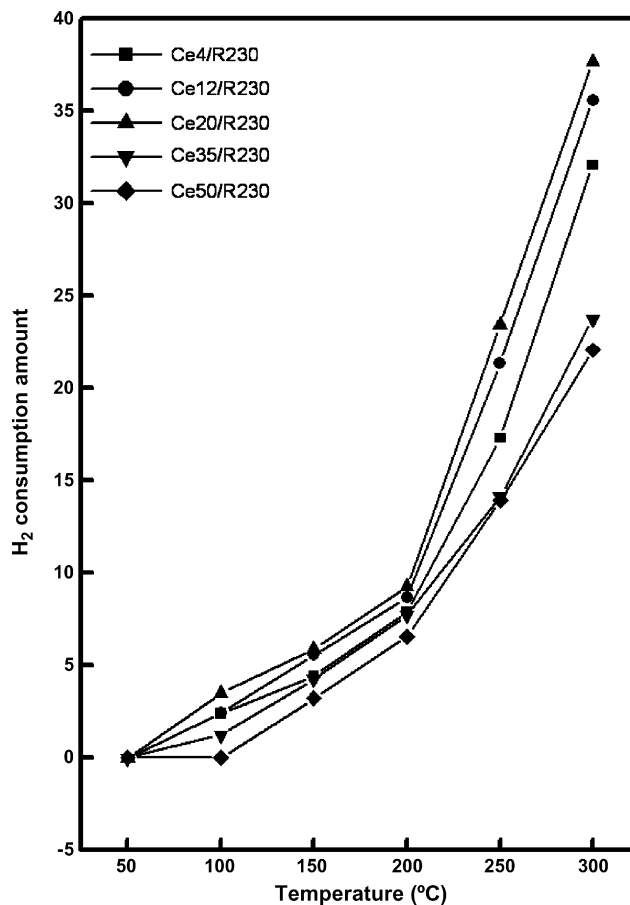


Fig. 3. The amounts of hydrogen consumption with the same temperature of CeX/R230 catalysts.

Ce35/R230 and Ce50/R230. Comparison with the theoretical values of  $\text{Co}_3\text{O}_4$  (0.33 and 1, respectively) that are based on Eqs. (1) and (2) also proved that the ceria can be reduced under lower temperature ( $T < 400\text{ }^\circ\text{C}$ ) over  $\text{CeX/R230}$  oxides. The higher dispersion of  $\text{CeX/R230}$  appears higher  $\alpha$  and  $\beta$  ratio that demonstrates the storing oxygen on ceria.

The specific feature of  $\text{Co}_3\text{O}_4$  is the self-assembly of nanoparticles to form a hollow spheroidal overlayers as observed in Fig. 4(a). The crystallite of a hollow spheroidal crystallite with an internal diameter of approximately 30–50 nm is mainly the Co-containing phase [29]. They are similar to the particles that had been observed earlier by Potoczna-Petru et al. [30]. When the cobaltic oxide has been modified with ceria, we can find that the surface of spheroidal crystallite is covered very uniform with highly ordered array as shown in Fig. 4(b) and (c). Not only increasing the dispersion of cobaltic oxide but decreasing the internal diameter (approached 15–25 nm) is observed in the Ce4/R230 and Ce20/R230 samples. While, the more ceria loading (i.e., Ce50/R230) encapsulates the cobaltic oxide that appears the characterization of ceria [see Fig. 4(d)]. Comparison of these results with the XRD and  $S_{\text{BET}}$  analysis suggest that the optimal ceria loading can increase both dispersion and surface area of catalyst and promote the catalytic activity.

Catalytic oxidation of carbon monoxide has attracted great interest in the recent decade because carbon monoxide is a well-known pollutant from automobile exhaust. Therefore, we pay

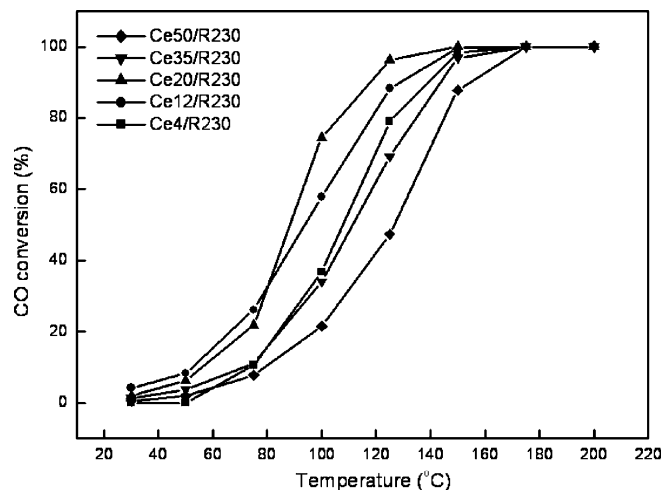


Fig. 5. Conversion profiles for CO oxidation over the  $\text{CeX/R230}$  catalysts: (a) Ce4/R230, (b) Ce12/R230, (c) Ce20/R230, (d) Ce35/R230 and (e) Ce50/R230.

attention to the abatement of carbon monoxide under low temperature. In order to test the catalytic activities of  $\text{CeX/R230}$  catalysts, light-off curves for CO oxidation are performed in a continuous flow micro-reactor to understand the effect of ceria loading. The catalytic activities for CO oxidation over  $\text{CeX/R230}$  catalysts are displayed in Fig. 5. The CO conversion over each sample generally increases with the reaction temperature.

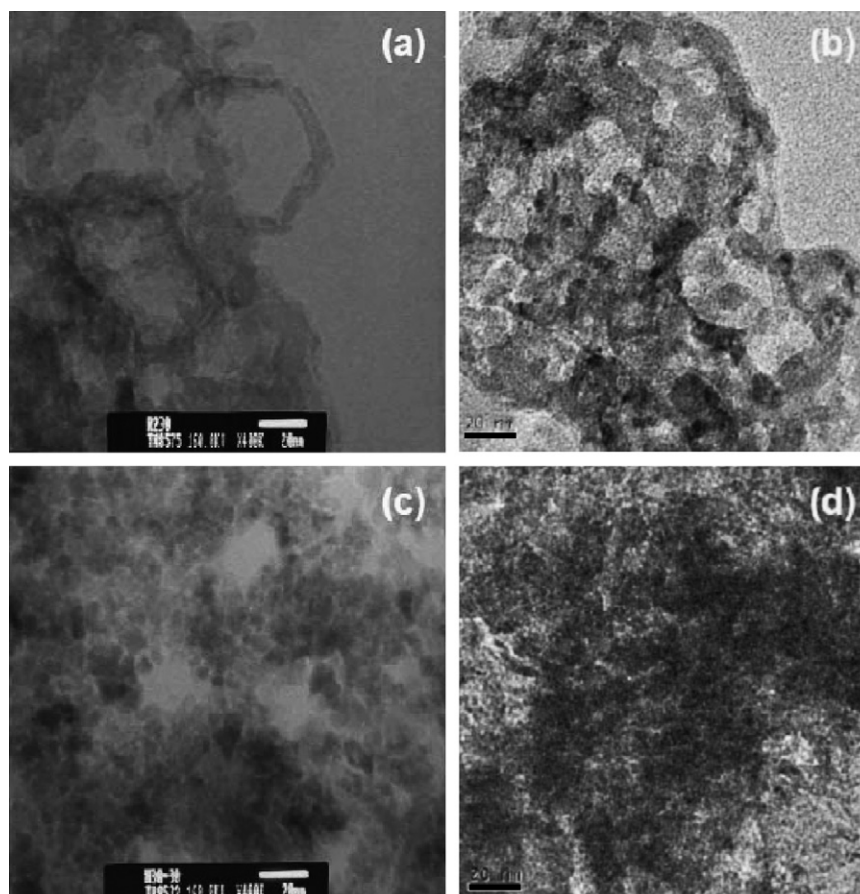


Fig. 4. TEM micrographs of (a) R230, (b) Ce4/R230, (c) Ce20/R230 and (d) Ce50/R230.

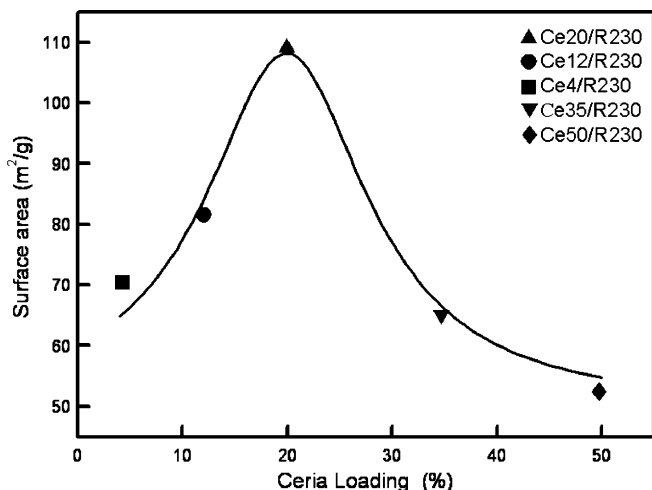


Fig. 6. The correlation of surface area with the  $T_{50}$  for CO oxidation over the  $CeX/R230$  catalysts.

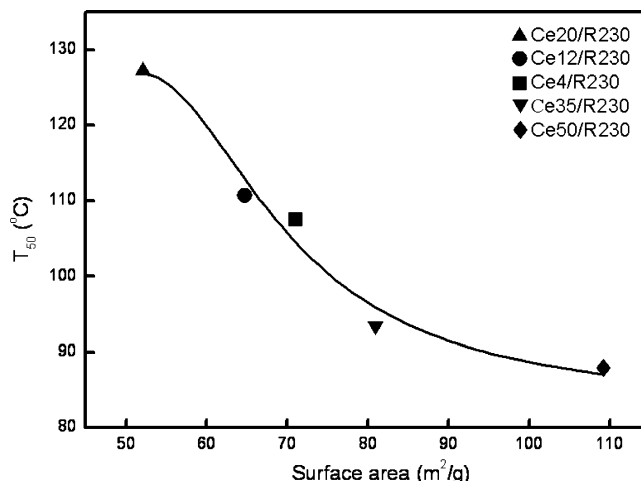


Fig. 7. The correlation of ceria loading with the surface area of the  $CeX/R230$  catalysts.

Evaluation of catalytic activity of each sample bases on the  $T_{50}$  (temperature for 50% CO conversion) and shows in the last column in Table 1. Apparently, the activity toward CO oxidation is promoted significantly by increasing the  $S_{BET}$  of catalyst. The correlation of surface area with the  $T_{50}$  for CO oxidation over the  $CeX/R230$  catalysts is shown in Fig. 6. Comparison with the TPR analysis, the slowly dropped  $T_{50}$  with increasing the  $S_{BET}$  of  $CeX/R230$  attributes mainly to the weakening of Co–O bonds that accelerates the desorption of oxygen from  $Co_3O_4$  [19]. The  $T_{50}$  decreases substantially by increasing the  $S_{BET}$ , i.e.,  $Ce20/R230$  ( $T_{50} = 88$  °C and  $S_{BET} = 109$   $m^2 g^{-1}$ ) >  $Ce12/R230$  ( $T_{50} = 93$  °C and  $S_{BET} = 81$   $m^2 g^{-1}$ ) >  $Ce4/R230$  ( $T_{50} = 108$  °C and  $S_{BET} = 71$   $m^2 g^{-1}$ ) >  $Ce35/R230$  ( $T_{50} = 111$  °C and  $S_{BET} = 65$   $m^2 g^{-1}$ ) >  $Ce50/R230$  ( $T_{50} = 127$  °C and  $S_{BET} = 52$   $m^2 g^{-1}$ ). The  $T_{50}$  of  $Ce20/R230$  catalyst is lower than 90 °C and converts completely around 150 °C. While, the  $T_{50}$  of  $Ce50/R230$  catalyst approaches 125 °C and converts completely over 175 °C. The stability of the catalytic activity under 150 °C over  $Ce20/R230$  catalyst maintains 100% conversion of CO after 48 h time-on-stream.

In the same, the correlation of ceria loading with the surface area of the  $CeX/R230$  catalysts is shown in Fig. 7. The less ceria loading cannot disperse effectively the cobaltic oxide whereas the more ceria loading encapsulates the cobaltic oxide that decreases both active sites and the  $S_{BET}$  of catalyst. The combined effect between cobaltic oxide and ceria can also be found from the tailing reduction of  $\beta$  peak as the ceria loading exceeds 20% [Fig. 2(e)–(g)] [23]. Compared the  $S_{BET}$  (the 2nd column of Table 1) of  $CeX/R230$  catalysts, the optimal ceria loading is 20%. Maybe some specific defect sites have been formed on the  $Ce20/R230$  catalyst that increases the  $S_{BET}$  and weaken the Co–O bond strength to promote the CO oxidation activity.

The rate of catalytic CO oxidation is also studied as a function of temperature. It is found that the rate of catalytic oxidation increases with the reaction temperature. The plots of  $\ln(dC/dt)$  versus  $1/T$  are found to be straight line for all samples

(Fig. 8). Activation energies ( $E_a$ ) of the reaction over  $CeX/R230$  catalysts are calculated according to the Arrhenius equation and shown in the 5th column of Table 1. Smit et al. [31] reported that the  $T_{50}$  around 100–170 °C for CO oxidation over Au/ $Fe_2O_3$  catalysts gave 13–25  $kJ mol^{-1}$  activation energies. For the Pt/ $CeO_2$ – $Al_2O_3$  catalysts, Oran and Uner [32] found that the  $T_{50}$  around 120–220 °C for CO oxidation gave 42–132  $kJ mol^{-1}$  activation energies. According to our results, the activation energies vary with the ceria loading that follow the order:  $Ce20/R230$  (10  $kJ mol^{-1}$ ) <  $Ce12/R230$  (18  $kJ mol^{-1}$ ) <  $Ce4/R230$  (26  $kJ mol^{-1}$ ) <  $Ce35/R230$  (30  $kJ mol^{-1}$ ) <  $Ce50/R230$  (55  $kJ mol^{-1}$ ). Especially for the  $Ce20/R230$  sample is better than the noble catalysts. Comparison of these results with the TEM analysis, suggest that the change of surface morphology can affect the rate of catalytic CO oxidation. The optimal ceria loading can increase both dispersion and surface area of catalyst and reduces the activation energies.

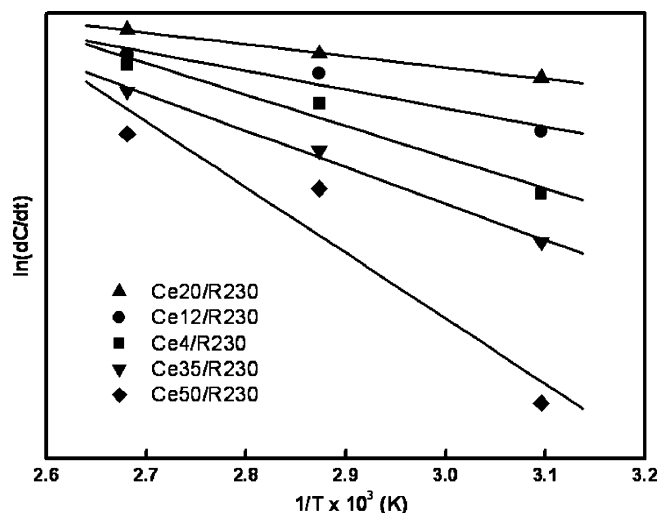


Fig. 8. Arrhenius plots for the rates of CO oxidation over  $CeX/R230$  catalysts.

#### 4. Conclusion

A series of CeX/R230 catalysts have been characterized and evaluated for CO oxidation. According to the results we find that the optimum loading of ceria is 20% (Ce20/R230). The Ce20/R230 sample exhibits highest surface area and best catalytic activity on CO oxidation ( $T_{50} = 88\text{ }^{\circ}\text{C}$ ) among these catalysts. We propose that the optimal ceria loading can increase both dispersion and surface area of catalyst and weaken the Co–O bond strength to promote the CO oxidation activity.

#### Acknowledgements

We are pleased to acknowledge financial supports for this study from Academia Sinica and the National Science Council of the Republic of China.

#### References

- [1] M.F. Luo, Y.J. Zhong, X.X. Yuan, X.M. Zheng, *Appl. Catal. A: Gen.* 162 (1997) 121.
- [2] S.D. Choi, B.K. Min, *Sens. Actuator B* 77 (2001) 330.
- [3] H. Arai, M. Machida, *Appl. Catal. A: Gen.* 138 (1996) 161.
- [4] S.A. Makhlouf, J. Magn. Mater. 246 (2002) 184.
- [5] Z.P. Hao, L.D. An, H. Wang, *Sci. China* 44 (2001) 596.
- [6] G.Y. Wang, H.L. Lian, W.X. Zhang, D.Z. Jiang, T.H. Wu, *Kinet. Catal.* 43 (2002) 433.
- [7] G.B. Hoflund, S.D. Gardner, *Langmuir* 2 (1996) 3431.
- [8] X. Tang, B. Zhang, Y. Li, Y. Xu, Q. Xin, W. Shen, *Catal. Today* 93 (2004) 191.
- [9] B. Skarman, D. Grandjean, R.E. Benfield, A. Hinz, A. Andersson, L.R. Wallenberg, *J. Catal.* 211 (2002) 119.
- [10] A. Martínez-Arias, M. Fernández-García, O. Gaálvez, J. Coronado, J. Anderson, J. Conesa, J. Soria, G. Munuera, *J. Catal.* 195 (2000) 207.
- [11] S.P. Wang, X.C. Zheng, X.Y. Wang, S.R. Wang, S.M. Zhang, L.H. Yua, W.P. Huang, S.H. Wu, *Catal. Lett.* 105 (2005) 163.
- [12] M.M. Mohamed, S.M.A. Katib, *Appl. Catal. A: Gen.* 287 (2005) 236.
- [13] R. Sasikala, N.M. Gupta, S.K. Kulshreshth, *Catal. Lett.* 71 (2001) 69.
- [14] F. Grillo, M.M. Natile, A. Glisenti, *Appl. Catal. B: Environ.* 48 (2004) 267.
- [15] M. Kang, M.W. Song, C.H. Lee, *Appl. Catal. A: Gen.* 251 (2003) 143.
- [16] J. Jansson, A.E.C. Palmqvist, E. Fridell, M. Skoglundh, L. Österlund, P. Thormhlen, V. Langer, *J. Catal.* 211 (2002) 387.
- [17] J. Jansson, *J. Catal.* 194 (2000) 55.
- [18] E. Gulari, C. Güldür, S. Srivannavit, S. Osuwan, *Appl. Catal. A: Gen.* 182 (1999) 147.
- [19] C.B. Wang, C.W. Tang, S.J. Gau, S.H. Chien, *Catal. Lett.* 101 (2005) 59.
- [20] J.J. Shao, P. Zhang, X.F. Tang, B.C. Zhang, W. Song, Y.D. Xu, W.J. Shen, *Chin. J. Catal.* 27 (11) (2006) 937.
- [21] J.J. Shao, P. Zhang, X.F. Tang, B.C. Zhang, J.L. Liu, Y.D. Xu, W.J. Shen, *Chin. J. Catal.* 28 (2) (2007) 163.
- [22] M. Haneda, Y. Kintaichi, N. Bion1, H. Hamada, *Appl. Catal. B: Environ.* 46 (2003) 473.
- [23] C.W. Tang, C.C. Kuo, M.C. Kuo, C.B. Wang, S.H. Chien, *Appl. Catal. A: Gen.* 309 (2006) 37.
- [24] H.K. Lin, H.C. Chiu, H.C. Tsai, S.H. Chien, C.B. Wang, *Catal. Lett.* 88 (2003) 169.
- [25] P. Arnoldy, J.A. Moulijn, *J. Catal.* 93 (1985) 38.
- [26] G.R. Rao, H.R. Sahu, B.G. Mishra, *Colloids Surf. A220* (2003) 261.
- [27] X.C. Zheng, S.P. Wang, X.Y. Wang, S.R. Wang, X.G. Wang, S.H. Wu, *Mater. Lett.* 59 (2005) 2769.
- [28] H.Y. Lin, Y.W. Chen, *Mater. Chem. Phys.* 85 (2004) 171.
- [29] C.B. Wang, H.K. Lin, C.W. Tang, *Catal. Lett.* 94 (2004) 69.
- [30] D. Potoczna-Petru, J.M. Jablonski, J. Okal, L. Krajczyk, *Appl. Catal. A: Gen.* 175 (1998) 113.
- [31] G. Smit, N. Strukan, M.W.J. Cráj, K. Lázár, *J. Mol. Catal. A* 252 (2006) 163.
- [32] U. Oran, D. Uner, *Appl. Catal. B: Environ.* 54 (2004) 183.